Journal of Applied Physics

Modification of energy band alignment and electric properties of $Pt/Ba_{0.6}Sr_{0.4}TiO_3/Pt$ thin-film ferroelectric varactors by Ag impurities at interfaces

Cite as: J. Appl. Phys. **115**, 243704 (2014); https://doi.org/10.1063/1.4885880
Submitted: 22 May 2014 • Accepted: 18 June 2014 • Published Online: 26 June 2014

S. Hirsch, P. Komissinskiy, S. Flege, et al.

JOURNAL OF APPLIED PHYSICS **115**, 243704 (2014)

Modification of energy band alignment and electric properties of $Pt/Ba_{0.6}Sr_{0.4}TiO_3/Pt$ thin-film ferroelectric varactors by Ag impurities at interfaces

S. Hirsch, P. Komissinskiy,[a] S. Flege, S. Li, K. Rachut, A. Klein, and L. Alff
Institute of Materials Science, Technische Universität Darmstadt, 64287 Darmstadt, Germany

(Received 22 May 2014; accepted 18 June 2014; published online 26 June 2014)

We report on the effects of Ag impurities at interfaces of parallel-plate $Pt/Ba_{0.6}Sr_{0.4}TiO_3/Pt$ thin film ferroelectric varactors. Ag impurities occur at the interfaces due to diffusion of Ag from colloidal silver paint used to attach the varactor samples with their back side to the plate heated at 600–750 °C during deposition of $Ba_{0.6}Sr_{0.4}TiO_3$. X-ray photoelectron spectroscopy and secondary ion mass spectrometry suggest that amount and distribution of Ag adsorbed at the interfaces depend strongly on the adsorbent surface layer. In particular, Ag preferentially accumulates on top of the Pt bottom electrode. The presence of Ag significantly reduces the barrier height between Pt and $Ba_{0.6}Sr_{0.4}TiO_3$ leading to an increased leakage current density and, thus, to a severe degradation of the varactor performance. © *2014 AIP Publishing LLC*. [http://dx.doi.org/10.1063/1.4885880]

I. INTRODUCTION

Parallel-plate thin film ferroelectric varactors are considered for tunable devices in microwave applications. The capacitance of the varactors is tuned by electric field utilizing the tunability of the permittivity of the dielectric layer. A solid solution $Ba_xSr_{1-x}TiO_3$ (BST) is widely used as a dielectric layer, where a high tunability of permittivity is achieved at room temperature, e.g., at $x = 0.6$.[1] Along with the quality of the dielectric layer, the performance of the varactors, e.g., tunability, high frequency dielectric losses, leakage current, and cycling stability, is strongly influenced by the used metal electrodes and the quality of the dielectric-metal interfaces.[2] Pt electrodes are commonly used in BST-based varactors due to their chemical stability and the high electric conductivity of Pt. Schottky-emission of electrons over the potential barrier at the BST/Pt interface is one of the physical mechanisms determining the electric losses and non-linear leakage current in the ferroelectric varactors. The reported small leakage current in BST varactors with Pt electrodes of about 6×10^{-5} A/cm^2 at 0.7 MV/cm is considered as an important advantage as compared to semiconductor devices.[2] The height of the Pt/BST Schottky barrier varies in a broad range between 0.4 and 1.6 eV depending on sample preparation.[3] In particular, the low Schottky barrier is attributed to oxygen vacancies formed in the BST films in the vicinity of the reduced Pt/BST interface.[3,4] Along with the influence of oxygen vacancies, the properties of the varactors are changed by defects and inhomogeneities in their microstructure and the presence of dopants and impurities.

Earlier, a beneficial effect of Ag doping was observed in high temperature superconductors, e.g., $YBa_2Cu_3O_x$ and $NdBa_2Cu_3O_x$, where improvement in the microstructure and rise of the superconducting critical current density was achieved.[5,6] Enhancement of dielectric properties with Ag-doping was demonstrated in Ag-BST ceramic composite[7] and Ag-doped BST thin films deposited by pulsed laser deposition[8] and sol-gel coating techniques.[9] The positive effect of Ag doping is attributed to the following two processes: (i) stronger oxygenation of the BST films by additional supply of more reactive atomic oxygen by metastable volatile AgO species reducing the amount of oxygen vacancies;[8] (ii) stronger pinning of domain walls in the presence of silver impurities.[8,10] The latter process was suggested as origin of the small leakage current measured in Ag/Ag-BST/$LaNiO_3$/$LaAlO_3$ varactors explained within the space-charge limited current model.[8] However, the effects of Ag-doping on chemical composition and height of the potential barriers at the interfaces of thin-film ferroelectric varactors have not been investigated in the previous studies.

Here, we report on the effect of Ag impurities on the electric properties of the Pt/BST/Pt varactors. As Ag is adsorbed at the Pt surfaces of the varactors, the height of the Pt/BST barrier is reduced and the leakage current is increased.

II. EXPERIMENTAL DETAILS

Varactor heterostructures were fabricated in parallel-plate geometry on (001) $SrTiO_3$ (STO) and Nb-doped (0.05 wt. %) (001) STO (STO:Nb) single-crystal substrates with a size of $5 \times 5 \times 0.5$ mm. Prior to the experiments, the substrates were chemically treated and annealed in oxygen resulting in a TiO_2-terminated surface with one-unit-cell terraces.[11,12] The treatment is also essential to remove surface contaminations with residual Si, which is typically observed in commercially available STO substrates after polishing.

A 150 nm thick Pt bottom electrode was deposited at room temperature by DC magnetron sputtering in argon atmosphere. Subsequently, a 200 nm thick BST ($x = 0.6$) layer was grown by pulsed laser deposition with KrF excimer laser (248 nm) at 0.3 Torr oxygen pressure and a substrate temperature of 600–750 °C.[13] The BST films grown on Pt are polycrystalline with preferential (110) orientation.

[a]Author to whom correspondence should be addressed. Electronic mail: komissinskiy@oxide.tu-darmstadt.de

Finally, a 200 nm thick Pt top layer was deposited by PLD at 500 °C and 0.15 Torr argon pressure. The geometry of the Pt/BST/Pt varactors was formed using stainless steel shadow masks during deposition of BST and the top Pt layers. Pt/BST/Pt varactors with diameters of the top Pt electrodes between 50 and 400 μm were fabricated (Fig. 1).

During the high-temperature fabrication steps of the varactors (e.g., deposition of the BST films), the samples were attached with their back side to 1 mm thick stainless steel plates using commercially available Pelco® colloidal silver paint by Ted Pella Inc. (Ag-glue). The back side of the stainless steel plates was heated using an infrared laser diode. Ag-glue has a high thermal conductivity and is often used in UHV physical vapor deposition systems for heat transfer from heater blocks towards samples.[14] Our investigation of the samples fabricated with Ag-glue reveals doping of the varactor heterostructures with Ag, which is diffused from Ag-glue at high temperatures required for deposition of BST. For comparison, several samples with Pt/BST/Pt varactors were fabricated using direct heating of the back side of the substrates by infrared laser beam without using Ag-glue. STO and Nb-doped STO substrates used in our experiments absorb energy at 938 nm wavelength of the laser diode and, thus, the samples can be directly heated.

Our surface composition analysis is based on X-ray Photoelectron Spectroscopy (XPS) data measured with monochromatic Al $K\alpha$ radiation using a Physical Electronics PHI-5700 spectrometer. The experimental energy resolution of the spectrometer of 0.4 eV was determined from the Gaussian broadening of the Fermi edge of a sputter cleaned Ag reference sample. Binding energies of the measured spectra were referenced with respect to the Ag Fermi edge and Ag $3d_{5/2}$ emission of the reference sample. A carbon C1*s* emission was always observed in the measured XPS spectra of the samples exposed to air. The binding energy of the C1*s* emission was estimated as 284.8 eV, which is typical for adventitious carbon and corresponds to the values reported in the literature.[15] No surface charging was observed during the XPS measurements of the STO/Pt/BST and STO:Nb/BST samples, because all the BST films were deposited on conductive Pt and STO:Nb layers and had a relatively low thickness. For the XPS measurements, the conductive STO:Nb and Pt layers of the samples were electrically grounded.

The composition depth profiles of the varactor heterostructures are acquired at several positions of each sample by Secondary Ion Mass Spectrometry (SIMS) using a Cameca ims 5f with cesium ion beam (Cs^+) at 14.5 keV and 15 nA. The beam was raster scanned over 150 × 150 μm, while negatively charged secondary ions from the inner 60 μm sputtered area were collected. Leakage current of the varactors was measured at room temperature with a *Keithley 2602* source meter, which has accuracy in the picoampere range.

III. RESULTS AND DISCUSSION

XPS survey spectra of two 150 nm thick Pt films deposited by DC magnetron sputtering on (001) $SrTiO_3$ substrates (STO/Pt) are shown in Fig. 2. After Pt deposition, both films were heated up to temperatures typical for BST film growth (600–750 °C) and annealed at these temperatures for 1 h. After the annealing step, the samples were *ex situ* transferred into the XPS chamber and the XPS spectra were measured at room temperature. The survey spectrum presented in curve (a) of Fig. 2 was measured for a sample directly heated during the annealing step from the back side by the infrared laser beam without use of Ag-glue. C1*s*, O1*s*, O KLL, and multiple Pt emissions are seen in the spectrum, where the emission lines of carbon and oxygen originate from hydrocarbon contaminations adsorbed at the surface of the sample exposed to atmosphere. The survey spectrum of the STO/Pt sample heated during the annealing step using Ag-glue is shown in curve (b) of Fig. 2. Ag 3*d*, Ag 3*p*, and Ag MVV emission lines are clearly visible in this spectrum in addition to the emissions observed in Fig. 2 curve (a). The inset in Fig. 2 shows Ag 3*d* emissions for this sample recorded with high resolution, where Ag $3d_{5/2}$ is observed at 368.2 eV typical for metallic Ag.[15]

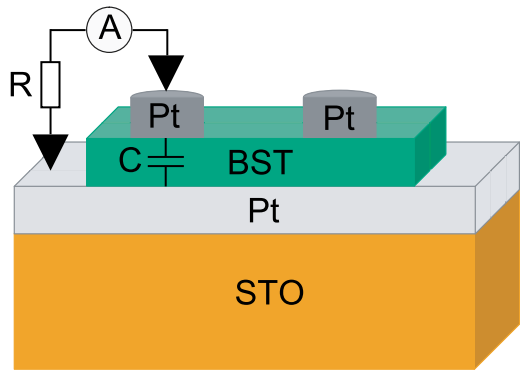

FIG. 1. Schematic drawing of $Pt/Ba_{0.6}Sr_{0.4}TiO_3/Pt$ (Pt/BST/Pt) varactors on a $SrTiO_3$ substrate with the circular top Pt electrodes of 50 to 400 μm in diameter (section view). A diagram of the leakage current measurements with amperemeter (A) and resistor (R) is shown for the varactor (C).

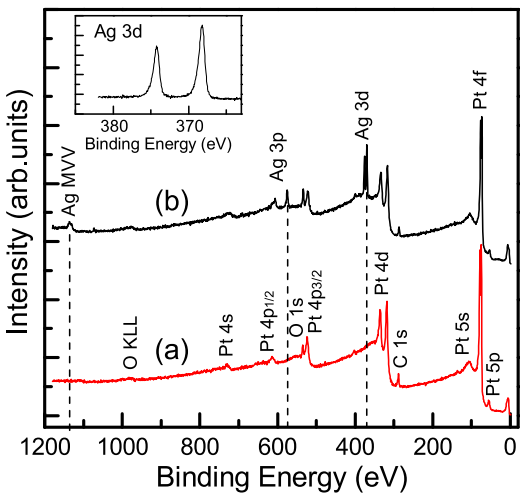

FIG. 2. XPS survey spectra recorded with monochromatic Al Kα radiation of 150 nm thick Pt films grown on $SrTiO_3$ substrates (STO/Pt) and later annealed at 750 °C for 1 h: (red curve (a)) XPS spectrum of the sample annealed using direct heating of the back side of the STO substrates with infrared laser beam; (black curve (b)) XPS spectrum of the sample annealed using Ag-glue on the back side of the STO substrates attached to the heated stainless steel plate. The inset shows the Ag 3*d* emissions recorded with high resolution for the STO/Pt sample annealed using Ag-glue.

Interestingly, the Ag emissions vanish from the XPS spectrum if a BST layer is deposited on top of Pt *in situ* after the annealing step. Moreover, no Ag emission lines are observed in the XPS spectrum of a bare STO substrate (not shown), which was heated up to 600–750 °C using Ag-glue indicating that the amount of Ag at the BST and STO surfaces is below the sensitivity of XPS. As the only possible source of Ag in our experiment is Ag-glue and no Ag emissions are observed in the spectrum of the directly heated STO/Pt sample, we conclude that at temperatures of 600–750 °C, Ag is diffused from Ag–glue and adsorbed preferentially on top of the Pt film rather than at the surface of BST or STO.

When using a more sensitive method (e.g., SIMS), Ag is detected also in all samples annealed using Ag-glue. In order to investigate the detailed distribution of Ag within the thin-film layers, we measured SIMS composition depth profiles of the STO:Nb/BST and STO/Pt/BST samples heated using Ag-glue during deposition of the BST films (see Fig. 3). The qualitative analysis of the Ag concentration in the samples is performed relative to the Ti signal with a constant intensity of 1.1×10^5 counts/s deep inside BST, STO, and STO:Nb. Positions of the interfaces between the materials in the depth profiles of the STO:Nb/BST and STO/Pt/BST samples are determined at half of the intensities of the Nb and Ti signals in Figs. 3(a) and 3(b), respectively, and marked in the graphs by full scale vertical dashed lines.

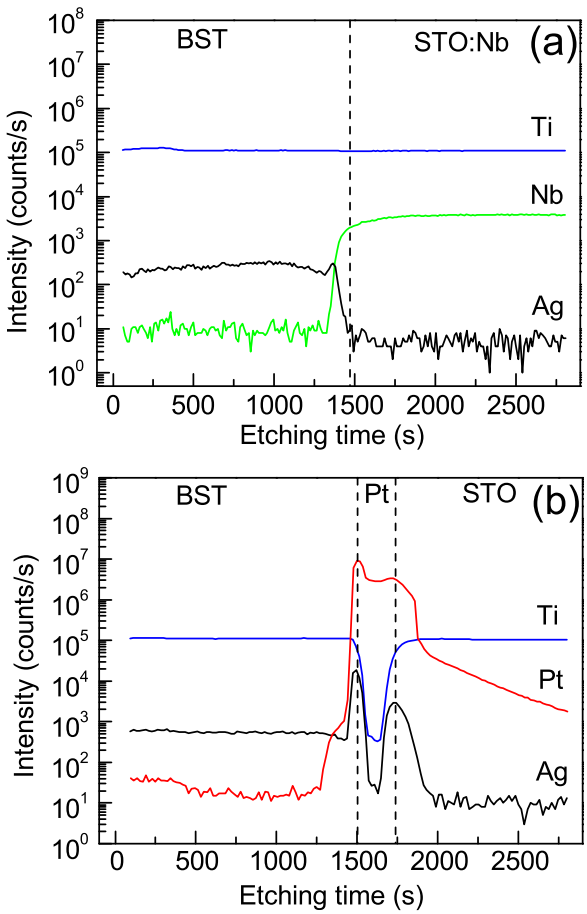

FIG. 3. SIMS composition depth profiles of the (a) $SrTiO_3$:Nb/$Ba_{0.6}Sr_{0.4}TiO_3$ (STO:Nb/BST) and (b) STO/Pt/BST samples recorded with cesium ion beam (Cs^+) at 14.5 keV and 15 nA. Both samples were heated using Ag-glue during deposition of the BST films. Full scale vertical dashed lines denote positions of the interfaces between the materials determined at half of the intensities of (a) Nb and (b) Ti signals.

A residual Pt signal with decreasing intensity is observed within the region of the STO substrate for the STO/Pt/BST sample (Fig. 3(b)). The signal can be attributed to some roughening of the surface during sputtering, influence of the crater walls due to the different charging levels of the layers during the measurement, and/or molecular interference because of the finite resolution of the mass spectrometer.

Deep within the STO and STO:Nb substrates, the signal denoted as Ag remains at a few counts per second level (etching time longer than 2500 s). As the Ag signal intensity is constant and no Ag is expected deep within the used STO and STO:Nb substrates, the observed Ag signal is probably caused by molecular interference. For the STO:Nb/BST sample, the Ag signal increases at the STO/BST interface towards the BST layer (Fig. 3(a)).

The depth profile of the Ag signal in the BST/Pt/STO heterostructure is more complex (Fig. 3(b)). A varying concentration of Ag is observed in the region of the Pt film, which is indicated by full scale vertical dashed lines in Fig. 3(b). The local minimum of the Ag signal in the Pt region reflects immiscibility of Ag and Pt in the bulk: the thermodynamic driving force biases the thermal diffusion in the direction of phase separation of Ag and Pt rather than intermixing in the bulk.[16,17] Thus, high concentration of Ag at the STO/Pt and Pt/BST interfaces results in two maxima of the Ag signal with intensities of 3.0×10^3 counts/s and 1.9×10^4 counts/s, respectively. The intensity of the Ag signal is stabilized at 6×10^2 counts/s inside the BST film of the STO/Pt/BST sample, which is much lower than at the maxima (Fig. 3(b)). The observed intensity of the Ag signal in the BST film of the STO:Nb/BST sample is approximately 3×10^2 counts/s, which is two times smaller than in the BST film of the STO/Pt/BST sample (Fig. 3). The concentration of Ag in BST is stable for both samples through the complete thickness of the BST layer.

Thus, the results of XPS and SIMS analysis indicate a higher concentration of Ag at the surfaces of Pt than inside the BST or STO layers. As there is no intermixing of Ag and Pt in the bulk, the Ag atoms diffused from the Ag-glue are accumulated at the Pt interfaces with BST and STO. Earlier tunnelling microscopy experiments at temperatures above 350 °C followed by theoretical modelling revealed formation of one-monolayer-thick two-dimensional alloy at the Pt/Ag interface.[16,17] It was shown that such surface-confined mixing is generally energetically favourable at the interfaces dominated by atomic size mismatch.[17]

Fig. 4 shows the valence band spectra of STO/Pt/BST heterostructures fabricated using direct heating and Ag-glue. The valence band maxima (VBM) are determined by linear extrapolation of the leading edge of the valence band emission with an uncertainty of ±0.1 eV due to the error in the calibration of the binding energy.[3] For the STO/Pt/BST heterostructures fabricated using direct heating (red circles in Fig. 4), the binding energy of the VBM relative to the Fermi energy is E_F–$E_{VB} = 2.4$ eV and corresponds to a position of the Fermi level deep within the BST band gap, which

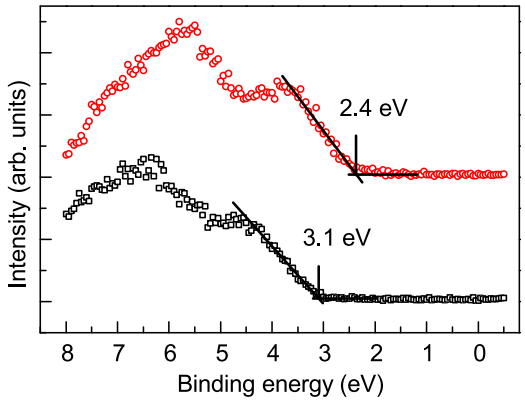

FIG. 4. Valence band spectra of $SrTiO_3$/Pt/$Ba_{0.6}Sr_{0.4}TiO_3$ (STO/Pt/BST) heterostructures fabricated using direct heating (red circles) and Ag-glue (black squares). The marked positions of the VBM are calculated by linear extrapolation of the leading edge of the valence band emission with an uncertainty of ±0.1 eV.

amounts to 3.2 eV.[3,18] For E_F–$E_{VB} = 2.4$ eV, the barrier height for electrons is 0.8 ± 0.1 eV, which is in reasonable agreement with values reported for oxygen deficient Pt/BST interfaces.[3] The binding energy of the VBM for the samples fabricated using Ag-glue is 3.1 eV (black squares in Fig. 4). For these samples, the barrier height is equal to only 0.1 eV, which is at the energy resolution limit of our experiments. Thus, the use of Ag in the fabrication process of the STO/Pt/BST heterostructures shifts the position of the Fermi level almost to the minimum of the BST conduction band resulting in direct injection of electrons into the BST. The corresponding energy band diagrams for the undoped and Ag-doped Pt/BST interfaces are shown in Figs. 5(a) and 5(b), respectively.

The low barrier height of 0.1 eV at the interfaces between BST and Pt should lead to a significant increase of the leakage current in Ag-doped Pt/BST/Pt ferroelectric varactors. Fig. 6 shows the electric field dependence of the leakage current density, $|J|$, of the Ag-doped and undoped Pt/BST/Pt varactors fabricated using Ag-glue (black squares) and direct heating of the samples by the laser diode (red circles), respectively. DC-biased Pt/BST/Pt varactors can be considered as two diodes in back-to-back geometry represented by the Pt/BST and BST/Pt bottom and top contacts, respectively. The current density is dominated by the

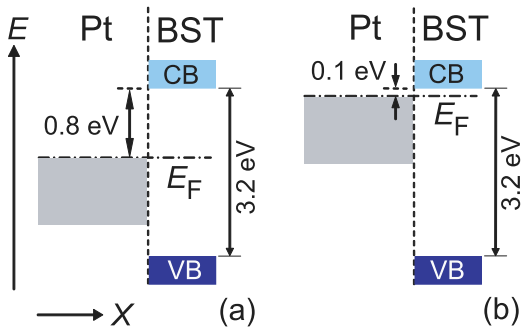

FIG. 5. Energy band diagrams experimentally determined for (a) undoped and (b) Ag-doped Pt/$Ba_{0.6}Sr_{0.4}TiO_3$ (Pt/BST) interfaces. Positions of the Fermi energy E_F relative to the BST band gap of 3.2 eV between valence band (VB) and conduction band (CB) are shown schematically.[18] The corresponding barrier heights between Pt and BST are (a) 0.8 eV and (b) 0.1 eV.

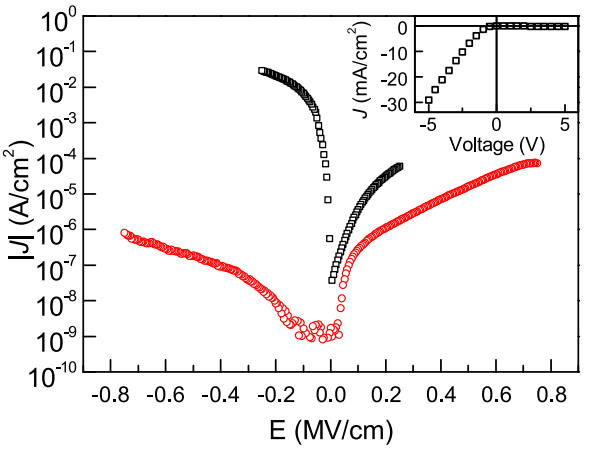

FIG. 6. Current density, log $|J|$, of (red circles) undoped and (black squares) Ag-doped Pt/BST/Pt varactors versus applied electric field E. The inset shows a highly asymmetric rectifying current-voltage (J-V) characteristic of the Ag-doped varactor.

negatively biased contact: either top BST/Pt interface or the bottom Pt/BST one. At zero bias, a small current density of $|J| \approx 1 \times 10^{-9}$ A/cm^2 corresponding to the resolution of the used current meter is observed for both Ag-doped and undoped varactors. The current density of the undoped Pt/BST/Pt varactors remains below 10^{-4} A/cm^2 for both positive and negative electric fields as high as 0.75 MV/cm (bias voltage of 15 V). The observed low current density of the undoped varactor indicates relatively high barriers for charge (electron) injection at the contacts between Pt and BST as shown in the corresponding band diagram (Fig. 5(a)). The Ag-doped varactor shows a highly asymmetric current-voltage (J-V) characteristic of rectifying shape (see inset in Fig. 6). The current density of the Ag-doped varactor measured with the top BST/Pt contact negatively biased at 5 V (positive $E = 0.25$ MV/cm in Fig. 6) is about 30 times higher than the one of the undoped varactor measured at the same bias. For the bottom Pt/BST contacts of the varactors negatively biased at 5 V (negative $E = -0.25$ MV/cm in Fig. 6), the ratio is increased from 30 up to 10^6 reflecting the higher concentration of Ag at the bottom Pt/BST interface than within the BST film (see SIMS data in Fig. 3).

IV. CONCLUSIONS

We have studied the effects of Ag impurities at interfaces of Pt/BST/Pt thin-film parallel-plate ferroelectric varactors. At sample temperatures of 600–750 °C as used for BST film growth by pulsed laser deposition, Ag diffuses from Ag-glue, which is utilized to improve the thermal contact between samples and the heater block. Phase separation of Ag and Pt, which are immiscible in bulk, leads to energetically favourable preferential precipitation of Ag at the surface of the bottom Pt layer of the varactors. The level of Ag doping of the BST layer yet detectable by SIMS is below the sensitivity of the used PHI-5700 X-ray photoelectron spectrometer. The Ag-doped Pt/BST interfaces are characterized by a low barrier height of 0.1 eV as compared to the one of 0.8 eV for undoped Pt/BST interfaces. The low barrier at the Ag-doped Pt/BST interface allows direct electron injection

from Pt into BST resulting in a high density of leakage current in varactors of up to 3×10^{-2} A/cm^2 at −0.25 MV/cm.

ACKNOWLEDGMENTS

This work was supported by the Deutsche Forschungsgemeinschaft within GRK 1037 (TICMO) and KO 4093/1-1.

[1]G. A. Smolenskii and V. A. Isupov, Zh. Tek. Fiz. **24**, 1375 (1954).
[2]S. Gevorgian, *Ferroelectrics in Microwave Devices, Circuits and Systems* (Springer-Verlag, London, 2009).
[3]R. Schafranek, S. Payan, M. Maglione, and A. Klein, Phys. Rev. B **77**, 195310 (2008).
[4]L. Alff, P. Komissinskiy, A. Radetinac, T. Sirman, and M. Vafaee, J. Phys. D: Appl. Phys. **47**, 034012 (2014).
[5]M. Lorenz, H. Hochmuth, D. Natusch, M. Kusunoki, V. L. Svetchnikov, V. Riede, I. Stanca, G. Kastner, and D. Hesse, IEEE Trans. Appl. Supercond. **11**, 3209 (2001).
[6]J. Kurian, H. Sato, T. Makimoto, and M. Naito, Appl. Phys. Lett. **87**, 022501 (2005).
[7]J. Q. Huang, Y. G. Cao, M. C. Hong, and P. Y. Du, Appl. Phys. Lett. **92**, 022911 (2008).
[8]A. Srivastava, D. Kumar, R. K. Singh, H. Venkataraman, and W. R. Eisenstadt, Phys. Rev. B **61**, 7305 (2000).
[9]K. P. Jayadevan, C. Y. Liu, and T. Y. Tseng, Appl. Phys. Lett. **85**, 1211 (2004).
[10]H. N. AlShareef, B. A. Tuttle, W. L. Warren, D. Dimos, M. V. Raymond, and M. A. Rodriguez, Appl. Phys. Lett. **68**, 272 (1996).
[11]M. Kawasaki, K. Takahashi, T. Maeda, R. Tsuchiya, M. Shinohara, O. Ishiyama, T. Yonezawa, M. Yoshimoto, and H. Koinuma, Science **266**, 1540 (1994).
[12]G. Koster, B. L. Kropman, G. Rijnders, D. H. A. Blank, and H. Rogalla, Appl. Phys. Lett. **73**, 2920 (1998).
[13]L. Alff, A. Klein, P. Komissinskiy, and J. Kurian, in *Ceramics Science and Technology: Synthesis and Processing*, edited by R. Riedel and I.-W. Chen (Wiley-VCH, Weinheim, 2012), Vol. 3, p. 267.
[14]P. Rundqvist, A. Vorobiev, S. Gevorgian, K. Khamchane, and Z. Ivanov, J. Appl. Phys. **93**, 1291 (2003).
[15]J. F. Moulder, W. F. Stickle, P. E. Sobol, and K. D. Bomben, *Handbook of X-Ray Photoelectron Spectroscopy: A Reference Book of Standard Spectra for Identification and Interpretation of XPS Data* (Physical Electronics, Inc., Minnesota, 1995).
[16]H. Roder, R. Schuster, H. Brune, and K. Kern, Phys. Rev. Lett. **71**, 2086 (1993).
[17]J. Tersoff, Phys. Rev. Lett. **74**, 434 (1995).
[18]M. Cardona, Phys. Rev. **140**, A651 (1965).